Mechanical properties of cold sintered ZnO investigated by nanoindentation and micro-pillar testing

Khushnuda Nur [a,b,c*], Muhammad Zubair[b,d], J S.K-L. Gibson[d], Stefanie Sandlöbes-Haut[d], Joachim Mayer[e,f,h], Martin Bram[a,g], Olivier Guillon[a,c,h]

[a] Forschungszentrum Jülich GmbH, Institute of Energy and Climate Research: Materials Synthesis and Processing (IEK-1), 52425, Jülich, Germany

[b] Department of Metallurgical and Materials Engineering, University of Engineering and Technology (UET) Lahore, Grand Trunk (GT) Road, Lahore, 54890, Pakistan.

[c] Rheinisch-Westfalische Technische Hochschule (RWTH) Aachen University, Institute of Mineral Engineering, 52064 Aachen, Germany.

[d] Institute for Physical Metallurgy and Materials Physics, Kopernikusstr. 14, RWTH Aachen University, 52074, Aachen, Germany.

[e] Central Facility for Electron Microscopy (GFE), RWTH Aachen University, Ahornstr. 55
52074 Aachen, Germany

[f] Ernst Ruska-Centre for Microscopy and Spectroscopy with Electrons (ER-C 2), Forschungszentrum Jülich 52425 Jülich, Germany

[g] Ruhr-Universität Bochum, Institut für Werkstoffe, Universitätsstraße 150, 44801 Bochum, Germany.

[h] Jülich Aachen Research Alliance, JARA-Energy, 52425 Jülich, Germany.

CRediT: Khushnuda Nur (Methodology, Validation, Formal analysis, Investigation, Writing – original draft), Muhammad Zubair (Methodology, Software, Writing – Review & Editing), J S.K-L. Gibson (Software, Resources, Data Curation, Writing – Review & Editing), Stefanie Sandlöbes-Haut (Resources, Writing – Review & Editing), Joachim Mayer (Resources, Writing – Review & Editing) Martin Bram (Supervision, Writing – Review & Editing), Olivier Guillon (Supervision, Project Administration, Funding Acquisition, Writing – Review & Editing)

Abstract

Characteristic densification in cold sintered microstructures could also have a strong influence in defining their mechanical response. For the first time, nanoindentation and micro-pillar testing is used to study these details. Based on our recent work, we selected cold sintered (250 ^{o}C, ~ 99 %

dense) and conventionally sintered (900 ^{o}C, ~ 98 % dense) ZnO samples. Hardness, elastic modulus and compressive stress of cold sintered samples were measured to be 5.5 GPa $\pm$ 0.5, 100 GPa $\pm$ 5 and ~ 1.2 GPa, respectively. Same values were observed almost comparable, for conventionally sintered ZnO as 4.8 GPa $\pm$ 0.6, 109 GPa $\pm$ 6 and 0.8 GPa, respectively. The distinctive nature of grain boundary regions in cold sintered samples were found to influence the deformation behavior of these samples, as confirmed by TEM investigations. Our study reveals the potential of cold sintering and use of selected testing techniques as suitable choice.

Keywords: Cold Sintering; stacking faults; amorphous regions; nanoindentation testing; micro-pillar testing.

* Corresponding author: k.nur@fz-juelich.de (Khushnuda Nur).

1. Introduction

Cold sintering is a new and highly promising method which enables one to densify materials at low temperatures. This technique has gained much interest in the materials community since the term “cold sintering process (CSP)” has been introduced by the research group of Randall´s group, in 2016. It utilizes an aqueous/liquid aid (deionized water, acetic aqueous solutions, organic solution, molten secondary phase etc.) combined with high external pressure to densify ceramic powder particles at minimum possible temperatures. [1][2][2][3][4][5] It has been successfully applied to many materials such as ZnO [6][7][8], ZrO_2 [9], MgO, V_2O_3, $BaTiO_3$, $NaNO_2$ [10], Li_2MoO_4, $BiVO_4$ [11][12][13][14], $LiFePO_4$ [15] etc. A lot of progress has been made to optimize the technique, however, there is still more to improve. One central aim is to improve the properties of these low temperature densified materials are associated with defects or amorphous regions at the grain boundaries. Electrical and electrochemical properties have already been investigated. [13][15][16][5] Nevertheless, investigation of the mechanical properties is still at an early state, but must be carefully considered to draw sound conclusions on the overall potential of the cold sintering process.

Up to now, upscaling of the cold sintering process has not been demonstrated yet. This restricts the preparation of samples with sufficient microstructural homogeneity suitable for reliable investigation of the mechanical properties by macroscopic methods like bending or tensile tests. In general, the systematic investigations of the mechanical properties of cold sintered samples raises some challenges. For example, cold sintered materials are usually characterized by nano-sized grains with defects originating from cold sintering like amorphous phases on grain boundaries or residual pores. [15][17] [7][18][19][20][21]

With respect to the current status of development, it is of general interest to better understand how low temperature sintered structures respond to mechanical load and how the specific processing influences this response. Due to the nano-size grained microstructure and the difficulty to prepare larger samples, we decided to apply nanoindentation and micro-pillar tests for studying the mechanical behavior and the related microstructural changes upon deformation. We are aware that these testing methods are usually favored for mechanical characterization of surface features, thin films, single grains of micrometer scale or selected phases within bulk samples. [22][23][24] (Nevertheless, our results show that both methods are suitable to gather novel insights how the

cold sintering alters deformation behavior in comparison to conventionally sintered samples. Before conducting the study, we optimized the cold sintering process in a way that the influence of processing related defects like residual pores were reduced to a minimum. Therefore, we believe that our results enable to draw first conclusions on how cold sintered microstructures – characterized by nanocrystalline grains, high volume fraction of grain boundaries and an amorphous phase on these grain boundaries as residual from cold sintering – specifically respond to mechanical load. With respect to literature, it is expected that due to this nanocrystalline nature significant change of mechanical properties can be expected compared to conventionally sintered samples.

In our study we chose ZnO as model material, which is well-known for its cold sintering ability and enables to produce almost dense samples at temperatures below 300°C and to reduce amorphous phases and pores to a minimum. [25] Lowum *et al.* [26], have studied the mechanical strength of cold sintered ZnO with the help of the ball-on-three-ball (B3B) biaxial bending testing method. The sample diameter was approximately 12.7 mm, the thickness ranged from 1.4 to 1.5 mm. For 97 % dense cold sintered ZnO, a characteristic strength of ~ 65 MPa and Weibull modulus of 8.2 was measured according to EN 843-5 standards, which was interpreted as poor mechanical strength associated with cold sintering. On the other hand, Gonzalez *et al.*, have calculated the stress exponent for cold sintered ZnO to be in the range of 2 – 4 and ascribed the possible active mechanisms as plastic deformation or grain boundary sliding. [8] Up to now, there is no information available in literature to what extent such mechanisms (e.g. dislocation formation) influence the deformation behavior of cold sintered samples.

As mentioned before, micromechanical testing, specifically, nanoindentation and micro-pillar compression, was used in the present study to investigate the mechanical response and to possibly predict the active deformation mechanisms of cold sintered materials. Nanoindentation is a testing method that is well-established in determining the hardness and elastic modulus of microstructural features on small scale, based on instrumented indentation depths typically of the order of a few hundred nanometers. [27] Here, we adapt the method for the characterization of the specific grain structure of cold sintered samples. Furthermore, nanoindents enable the deformed zone to be clearly identified in a subsequent TEM investigation. As a second method, micro-pillar compression testing has been selected to measure the compressive strength. This method was

introduced by Uchic and Dimiduk in 2005 to test micro – sized samples in uniaxial compression [28]. The plastic response of the samples under a compressive load is studied with the help of a stress-strain curve, generated by using a flat punch diamond indenter to compress a cylindrical specimen manufactured using focused ion beam machining. Although originally used to study the size effect in metals, it is now also widely applied to ceramic and other brittle materials. [29] There are several studies available in literature on nanoindentation of ZnO single crystals [30] [31] [32] and thin ZnO films [33] [34] [35] as well as on micro-pillar testing of ZnO [36][37][38]. However, to the best of our knowledge, neither of these methods have been applied to cold sintered materials, as has been carried out in this work.

In summary, the present study aims to demonstrate the potential of nanoindentation and micropillar tests for studying the response of cold sintered samples under mechanical loads. Both methods enabled us to draw first conclusions on the role of dislocations and stacking faults already formed during cold sintering on the deformation behavior. In this sense, we believe that the results are trend-setting for the cold sintering community, but scaling-up of technology and additional mechanical tests on a macroscopic level are necessarily required to come to sound conclusions regarding mechanical properties in the as cold sintered state. Such tests are part of our ongoing work.

2. Experimental work

2.1 Starting materials

ZnO dense pellets (cold sintered or conventionally sintered) were prepared from commercial ZnO powder delivered by Alfa Aesar (ThermoFischer GmbH, Kandel, Germany). According to the powder manufacturer it has the product number NanoArc ZN-0605 exhibiting 99 % purity and an average particle size of 40 – 100 nm. Cold sintering was performed inside a FAST/SPS device (HP-D5, FCT Systeme, Rauenstein, Germany) and hot worked steel tool die (W-360-Isobloc, Böhler, Germany). Parameters were used as, 250 ^{o}C, 300 MPa, 3.2 wt% of deionized water as an aqueous aid and a dwell time of 20 min. The effect of the atmosphere was studied by varying the atmosphere inside the FAST/SPS chamber. Therefore, three different atmospheres were used, vacuum, argon and air. For comparison, conventionally sintered ZnO sample has been prepared by using the same ZnO_40 – 100 powder. The parameters for conventional sintering were 900 ^{o}C, a dwell time of 60 min, and air atmosphere. Sintering was done in a muffle furnace (Nabertherm

furnace, L16/14, Germany). For more details on the sample processing, we refer to our recent work [25].

2.2 Transmission electron microscopy

The microstructure of the as-sintered samples was characterized in detail at Ernst Ruska Center (ERC, Forschungszentrum Jülich) by transmission electron microscopy (TEM) focusing mainly on the grain boundary regions. For this purpose, lamellae were prepared with the help of dual beam FIB-SEM (Focused Ion Beam – Scanning Electron Microscope) using a FEI Helios Nanolab 460F1 instrument (FEI Company Inc., Hillsboro, Orgeon, USA) [39] For TEM investigations, an FEI Titan Tecnai G2 F20 TEM [40] operated at 200 kV was used. Microstructure of samples deformed by nanoindentation was investigated at Gemeinschaftslabor für Elektronenmikroskopie (GFE, RWTH Aachen) using a FEI Strata 400 FIB workstation for preparation of lamellae at the flanks of the nanoindents and a FEI Tecnai F20 for TEM analysis

2.3 Ceramographic sample preparation

Before mechanical testing, the surface of the cold sintered samples was prepared by ceramographic methods. For nanoindentation testing, cold sintered and conventionally sintered samples were ground with emery paper to a 4000 grit finish. Grinding was carried out by holding the sample in hand while using an automatic grinding and polishing machine. This was found to be required to achieve a reliable surface quality. For micro-pillar testing, samples were ground to a 4000 grit finish followed by polishing using 3 μm and 1 μm diamond pastes, respectively. Here, the samples were inserted into sample holder of the automatic grinding and polishing machine.

2.4 Nanoindentation testing

Nanoindentation was performed using a Nanomechanics iNano indenter (TN, USA) equipped with a continuous stiffness measurement (CSM) unit. Two different types of tests were performed on all samples, i) nanoindentation constant strain rate (CSR) tests and ii) micro-pillar compression tests. In nanoindentation CSR testing, the samples were indented using a diamond Berkovich indenter tip provided by Synton MDP, Switzerland. The diamond area function (DAF) and frame stiffness were first calibrated on a polished aluminium sample at room temperature (keeping in mind the fact that elastic modulus of aluminium and of other standard calibration sample - fused silica – has only slight difference and ZnO is a soft ceramic). The reduced hardness of the

aluminium calibration sample with respect to fused silica allows calibration data to be obtained over the whole indentation depth (~1000 nm) which is otherwise not possible given the limit on the possible applied load. All tests (25 indents per sample) were performed at room temperature and at a strain rate of 0.2 s^{-1}. The samples were indented up to a maximum load of 45 mN. The maximum load was held constant for one second before unloading. Secondary electron (SE) images of the indents were taken using SEM Zeiss LEO 1530 (Zeiss, Oberkochen, Germany) and FEI 600i Helios Nanolab (FEI Company, USA).

2.5 Micro-pillar testing

Micro-pillars with nominal dimensions of 2 μm (diameter) and 4 μm (height) were produced using FIB milling using an FEI Helios Nanolab instrument at a current of 80 pA. The initial cuts for the pillars were made using a coarse beam current of 21 – 9.3 nA, followed by annular milling at a lower beam current of 0.79 nA. For the exact measurement of stress and strain, the actual diameter and length determined by secondary electron (SE) imaging in SEM were taken.

The micro-pillar compression tests were also done in the iNano indenter using a 10 μm diameter diamond flat punch provided by Synton MDP, Switzerland. Micro-pillars were compressed at a constant displacement rate of 10 $nm \cdot s^{-1}$ until fracture. In the present study, only the compressive strength was of interest for all samples to be tested. Therefore, associated limitations of the testing device (i.e. the feedback loop required to maintain a constant displacement rate in an intrinsically load-controlled machine) and the subsequent difficulty in studying post-yielding events such as strain bursts were avoided. Values showed here were an average of at least three values. When considering the small grain sizes of the cold sintered samples (113 nm $\pm$ 34, 103 nm $\pm$ 19 and 98 nm $\pm$ 34 in vacuum, argon and air atmospheres, respectively) the micro-pillars contained approximately 400 grains in the case of cold sintered samples and approximately 10 grains in the case of conventionally sintered samples (grain size of > 1 μm) (Figure 1). In both cases, there are likely sufficient grains that there is no strong influence of crystal anisotropy on the mechanical response. However, the increased number of tested grains in the cold sintered samples could influence the final measured values: both within the grains in terms of the role of long-range interactions between dislocations and related defects, or due to the fact there are an increased number of grain boundaries within the specimen.

The true strain was calculated from the corrected depth as according to Sneddon's correction [41].

$$\Delta x_{pillar} = \Delta x_{total} - \frac{(1-\nu_{sub}^2).f}{2E_{sub}r_{base}} - \frac{(1-\nu_{ind}^2).f}{2E_{ind}r_{top}} \quad \text{Eq 1}$$

Here, f is the applied force, ν_{sub} and ν_{ind} are the Poisson ratios of the substrate material (material under investigation: ZnO and the indenter, respectively, E_{sub} and E_{ind} are the Young's moduli of the substrate and the indenter, respectively, and r_{base} and $r_{top}$are the radii of the top and base of the pillars. The value of E_{ind} is taken as 1141 GPa and ν_{ind} as 0.07. [42][34], ν_{sub} it is assumed to be 0.35 [43] (E_{sub} were taken as 98 GPa, 100 GPa and 92 GPa for cold sintered ZnO pillars from the results of nanoindentation test).

3. Results

3.1 Cold sintered and conventionally sintered pellets

The cold sintered samples showed 98 – 99 % relative density with microstructures free from pores or holes and almost negligible effect of the applied atmosphere on cold sintered densification while conventionally sintered sample had ~ 98 % relative density. Selected cold sintered and conventionally sintered samples had a diameter of 12 mm and 20 mm and a height of 3.93 $\pm$ 0.09 mm and 1.846 $\pm$ 0.477 mm, respectively. Grain size measurement was carried out by image analysis (> 200 grains for each value). Fracture surface analysis by SEM in Figure 1 showing clearly the difference of grain sizes for both types of sintered samples.

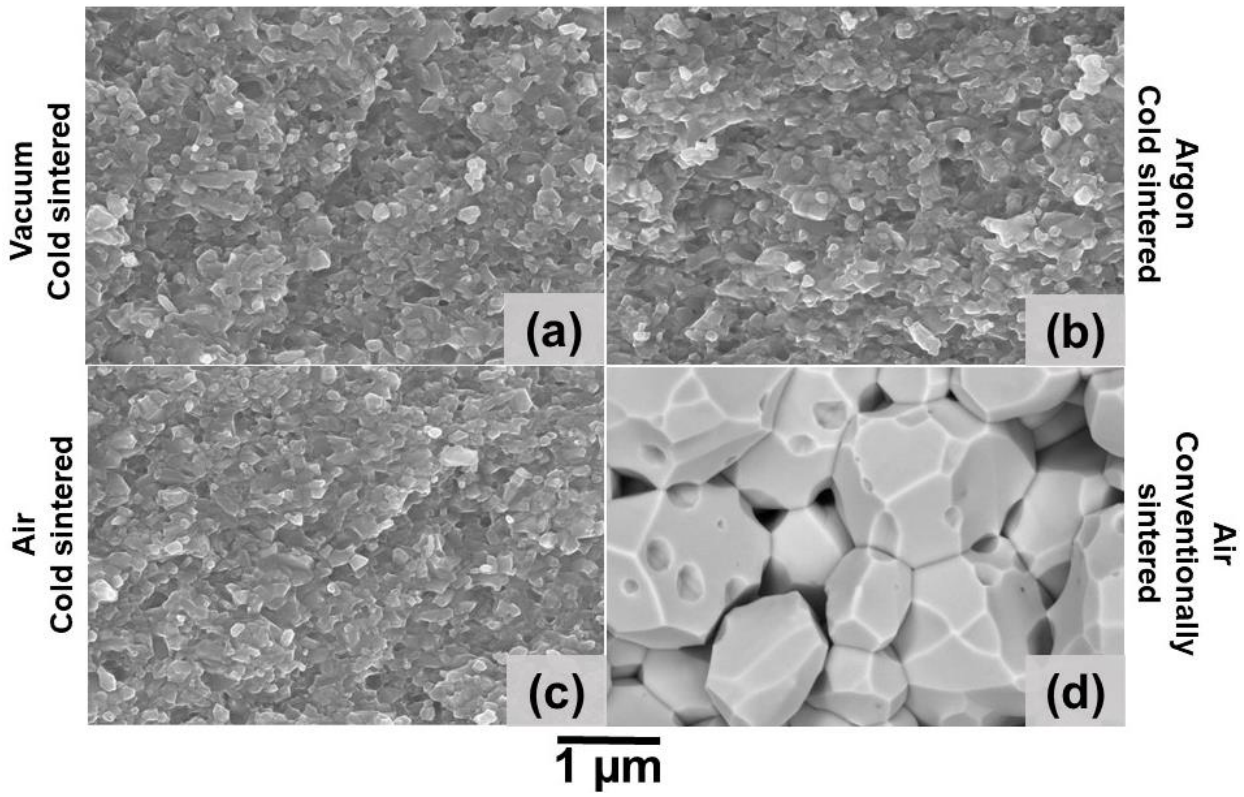

Figure 1. SEM micrograph of fracture surfaces of ZnO samples (a), (b) and (c) cold sintered in the atmospheres of vacuum, argon and air (250°C, 300 MPa, 20 min, density > 98%), respectively and (d) conventionally sintered in the atmosphere of air (900°C, 60 min, air, density 98 %).

3.2 TEM analysis of samples in the as cold sintered state

It has been confirmed in our previous study [44] that SEM analysis of fractured surfaces for ZnO, cold sintered in vacuum, argon and air atmosphere showed almost pore free grain boundary regions. Additionally, TEM analysis of one of these samples (in air cold sintered ZnO pellet) revealed that the grain boundary regions were observed to be free of pores. Though, a very thin bright region along the grain boundaries was identified as presumably amorphous phase. In the present study, a comparative TEM analysis has been made for pellets cold sintered in vacuum, argon and air. For cold sintered ZnO we have reported before that the final density and the densification behavior of these samples were not affected by the atmosphere in the FAST/SPS chamber.

Figure 2 shows the TEM analysis for cold sintered ZnO. In lower magnification (Figure 2 a, d, g), bright films are visible along the grain boundary that could be interpreted as pores or holes.

However, at higher magnification (Figure 2 b, e, h, c, f, i), it is evident that these areas are very thin (few nm) amorphous films that formed along the grain boundaries during cold sintering. Another important observation at higher magnification is the presence of defects such as dislocations and stacking faults already in the as cold sintered state. These defects are preferably located at or in the vicinity of grain boundaries. The obvious inhomogeneous distribution of stacking faults in the microstructure hints on differences of the strain energies probably caused by specific grain orientations and varying amount of amorphous phases at grain boundaries. TEM diffraction contrast of dark and bright fringes (specifically in Figure 2 c, f, i) also known as Moiré fringes shows the perfect crystal lattices laying over each other. While the offset observed in between these fringes is an indication of bended lattices, showing the presence of stacking faults.

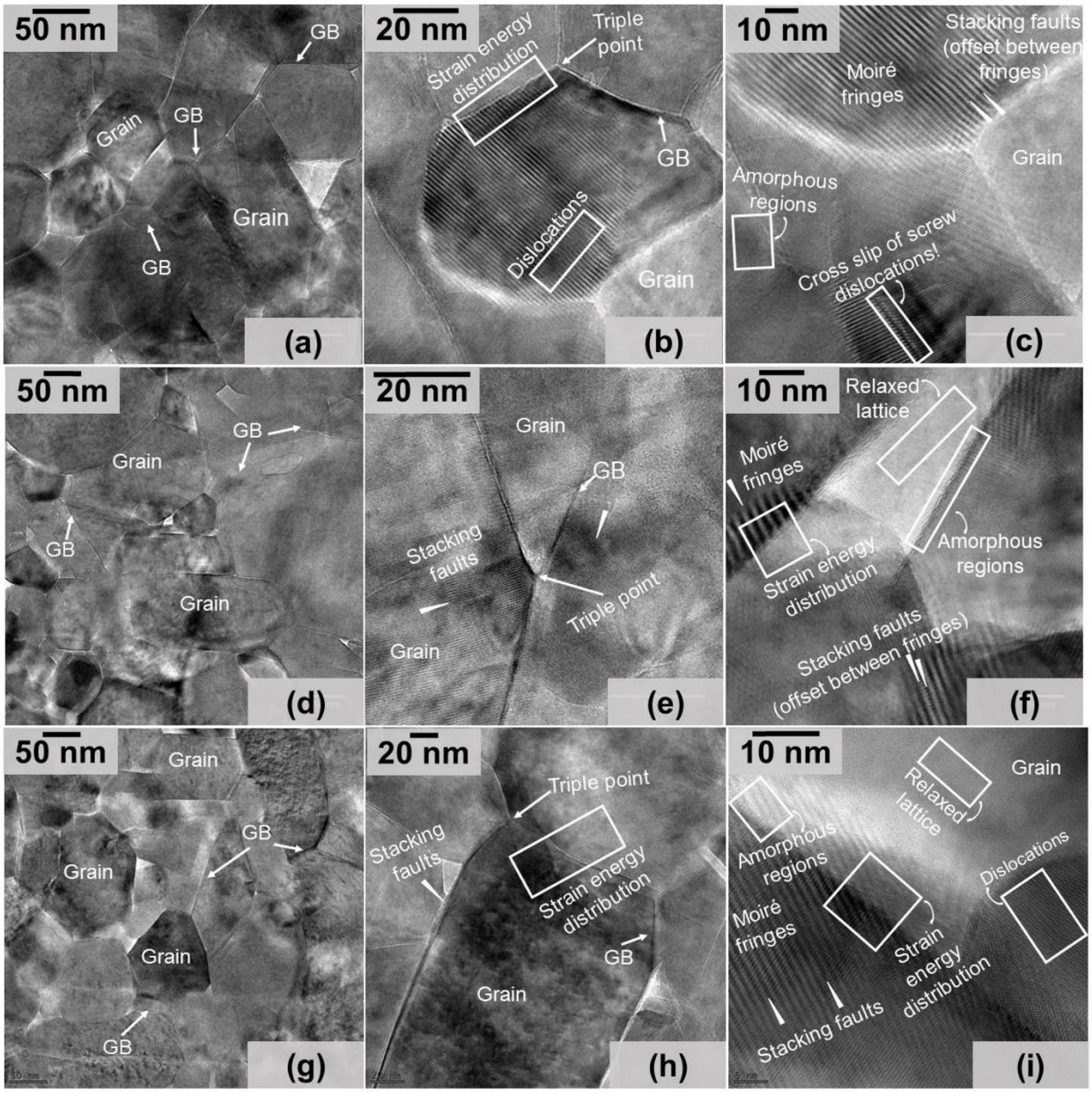

Figure 2. TEM analysis of ZnO: cold sintered in vacuum atmosphere (a, b and c), argon atmosphere (d, e and f) and air atmosphere (g, h and i).

3.3 Nanoindentation testing

Figure 3 shows SEM images of the residual imprints after Berkovich nanoindentation (cold sintered and conventionally sintered samples). These images are showing the nanoindents on the surface of the samples that were specifically prepared as described in the section 2.3. For samples prepared otherwise, by using automatic grinding and automated polishing it was almost impossible

to get to optimized surface finish as can be seen in Figure S 1 and Figure S 2. Specifically, for conventionally sintered sample, surface roughness was so intense (because of large size grain sizes) that most of the times the nanoindenter was going deep into the holes, making measurement highly unreliable (Figure S 1). In

Figure 3 a, b, c, pile ups are clearly visible around the indents in cold sintered samples independent of the atmosphere used during cold sintering which are not observable in Figure S 2. It must be considered that presence of pile ups indicates pronounced plastic deformation and enhanced fracture toughness. However, the increased contact area typically results in the calculated values of hardness and elastic modulus being overestimated compared to the true values. [45][23][46] This effect is minimised here as the mechanical data are taken from indentation depths below the final indentation depth, i.e. where the magnitude of the pile up is less significant than that observed in the SEM images. In contrast, the conventionally sintered ZnO shows no pile up, but cracks are visible along grain boundaries around the indents. To better understand this different behavior, microstructure of ZnO sample cold sintered in air and ZnO sample conventionally sintered was investigated by TEM. Therefore, FIB lamellae were prepared from the flanks of the nanoindents at the positions marked by a yellow bar in Figures 3c and 3d.

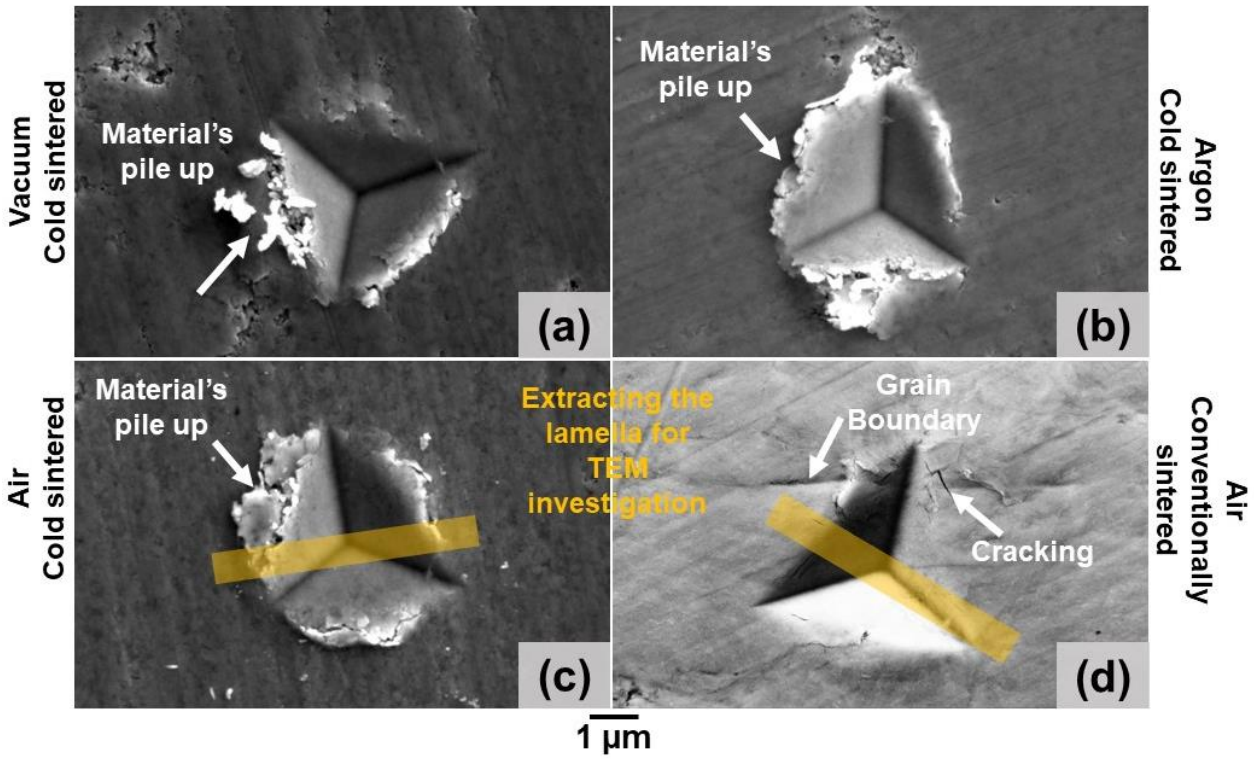

Figure 3. SEM micrographs of nanoindents on the surface of ZnO pellets, (a) cold sintered in vacuum atmosphere, (b) cold sintered in argon atmosphere and (c) cold sintered in air atmosphere, (d) conventionally sintered in air atmosphere (yellow strips in c and d show the areas, where FIB lamellae were prepared for TEM investigation).

Figure 4 shows representative load – depth, hardness – depth and elastic modulus – depth curves for eight tests performed on cold sintered samples processed in vacuum (a – c), argon (d – f) and air (g – i), respectively. The corresponding data for conventionally sintered ZnO are given in Figure 4 (j – l). Higher penetration depths were observed for indents performed on conventionally sintered samples in comparison to cold sintered samples. Further, during a holding period of one second at peak load, some creep deformation was observed as evident from the increase in the penetration depth of around ~ 40 nm during the holding period. The hardness and elastic modulus values at around 250 nm depth are shown in Figure 4 (b, e, h, k). Scatter associated with the results of conventionally sintered ZnO, although very small, but could be originating from crystallographic orientations. Some indents reveal pop-in events in the load – penetration curves (Figure 4 a, d, g, j). A pop-in event is a sudden increase in penetration depth during loading. In the present study, pop-in events have been observed for only few indents independent of the applied load (Figure 4 a, d, g, j and supplemental Figure S 3).

Figure 5 shows the average hardness and elastic modulus values at a depth of 500 nm, the error bars show the standard deviation. The cold sintered samples show that the sintering atmosphere induces only a negligible effect of sintering atmosphere on the mechanical properties is observed. However, the values of hardness for cold sintered ZnO in contrast to the conventionally sintered sample indicates the difference of homogeneity in both samples. Cold sintered samples offered more of homogenous regions to be covered by the indenter as compared to that provided by conventionally sintered samples.

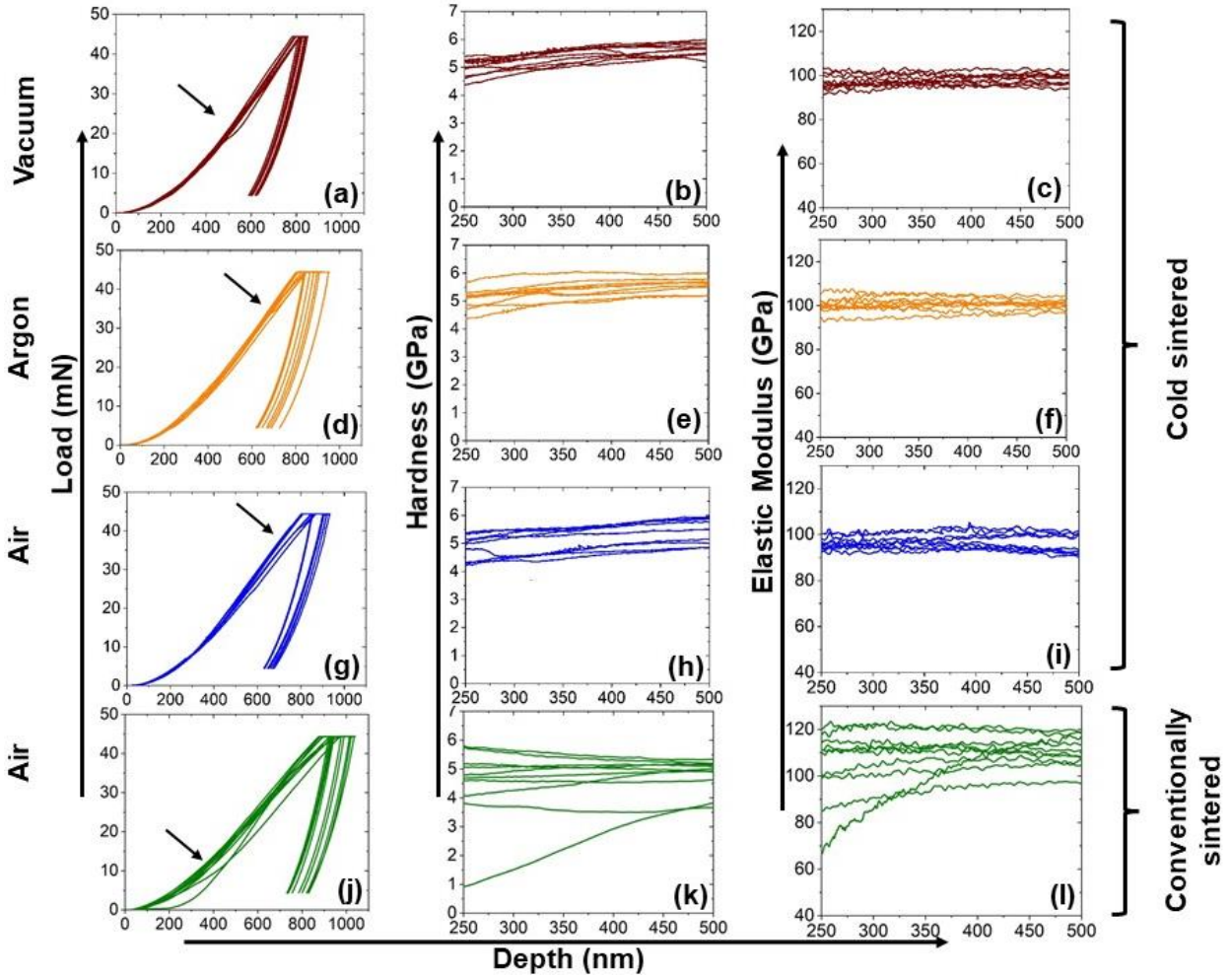

Figure 4. Nanoindentation testing of cold sintered samples and conventionally sintered sample: Load – depth curves (a, d, g), hardness – depth curves (b, e and h) and modulus – depth curves (c, f and i) for respective atmospheres.

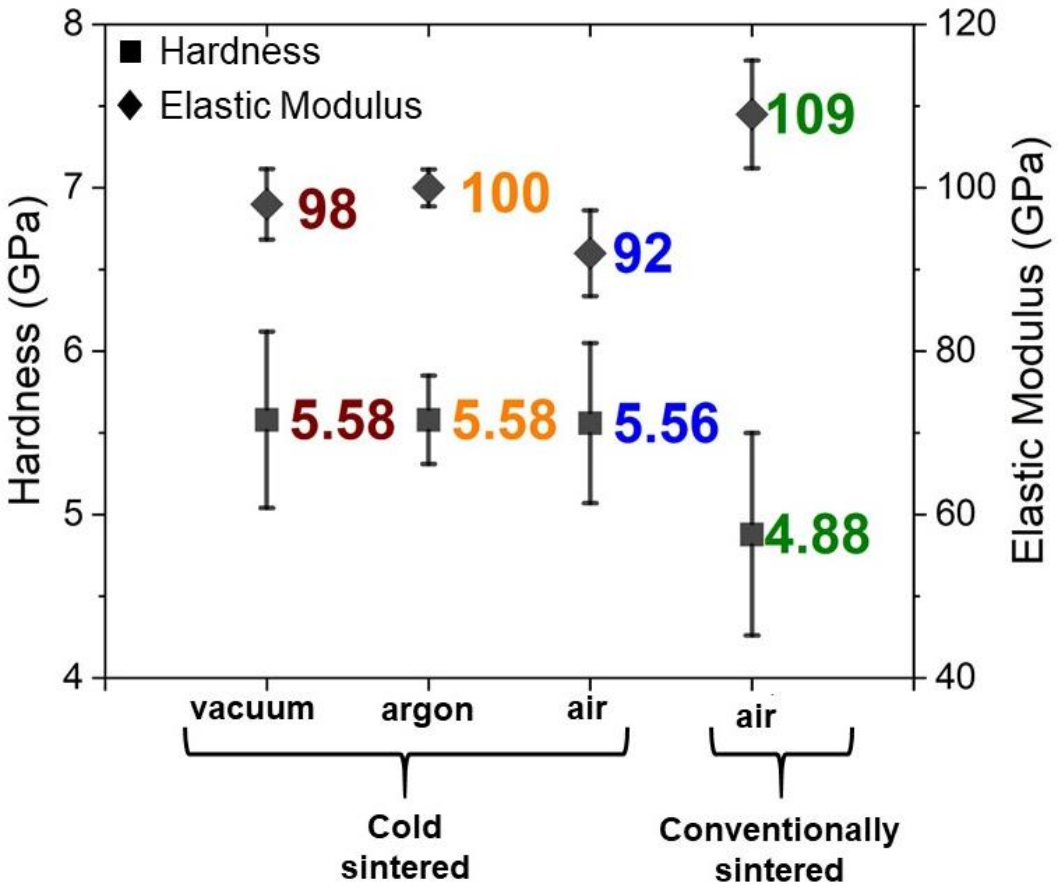

Figure 5. Average values of hardness and elastic modulus for cold and conventionally sintered ZnO samples.

Further, it can be seen from the Figure 5, that the elastic modulus of fine grained cold sintered ZnO is slightly lower than that of the coarse grained conventionally sintered ZnO. The modulus, in nano materials, generally decreases decreasing grain size. [47] [48][49][50][51][52][53][54] This effect becomes more intense for finer sizes (< 20 nm). [55]

3.4 Micro-pillar testing

Figure 6 shows SEM images of FIB milled micro-pillars prepared from cold sintered and conventionally sintered samples. Figure 6 a, c, e and g show the as-milled micro-pillars and Figure 6 b, d, f and h, the compressed micro-pillars. Figure 7 shows the corresponding stress – strain curves. The maximum compressive stresses were accordingly calculated as ~ 1.2 GPa for cold sintered ZnO and ~ 0.8 GPa for conventionally sintered ZnO, Figure 7. The non-linear portions in the stress-strain curve at the beginning of compression are caused by the limited contact of indenter

and pillar (effect of surface roughness). Therefore, the elastic moduli were not calculated from the micro-pillar compression tests but the values obtained from nanoindentation were used instead. The oscillations seen in the stress-strain curves (Figure 7) are resulting from feedback loops (a limitation of the device) as loading was done at a constant average displacement rate, therefore other features such as strain bursts and yielding were difficult to observe.

The true compressive strengths of all cold sintered samples are very similar (~ 1.2 GPa) while that of the conventionally sintered sample significantly lower (~ 0.8 GPa). This low compressive strength is assumed to result from large residual pores in between coarse grains (Figure 1 d and Figure 6 g) leading to intergranular fracture (Figure 6 h).

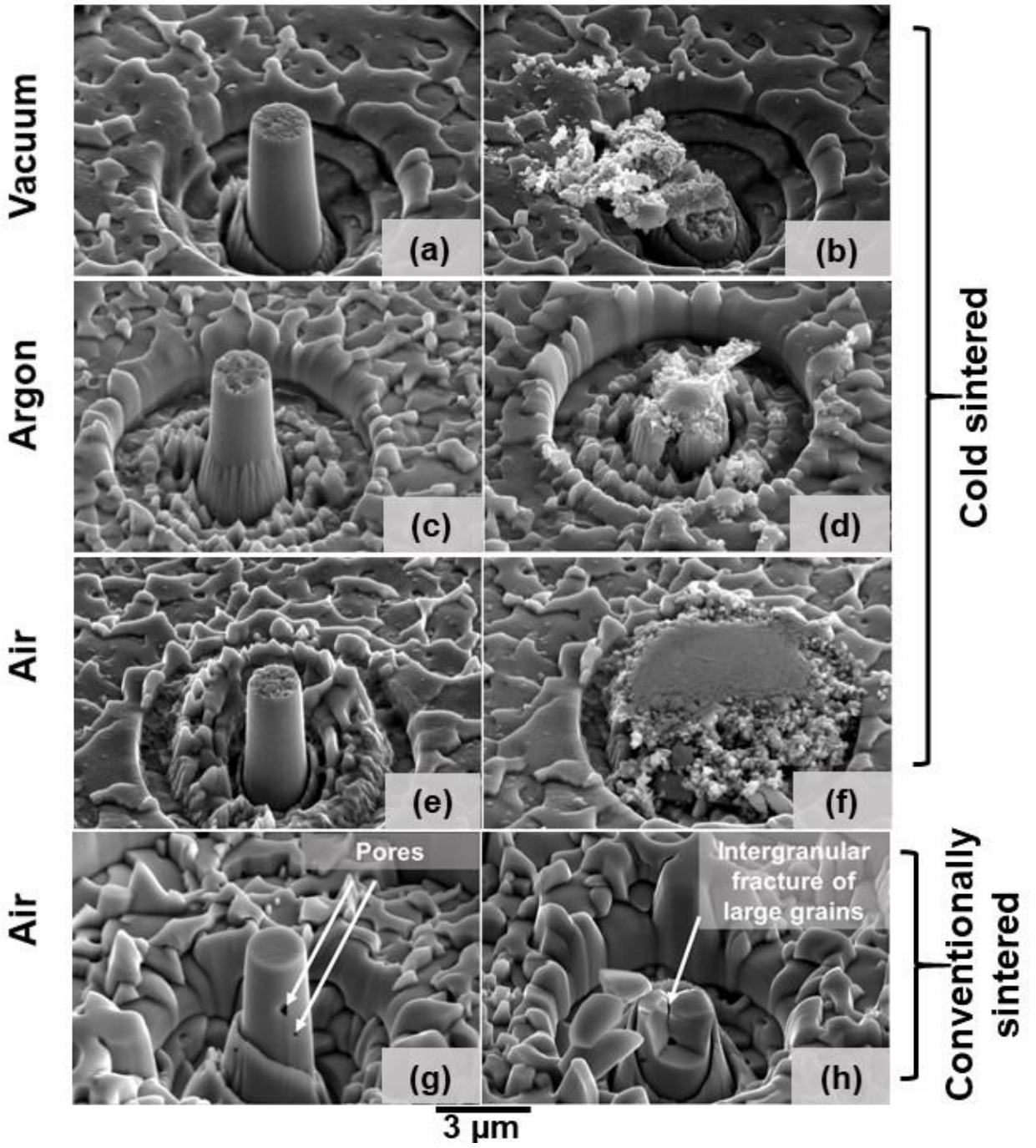

Figure 6. (a, c, e, g) FIB milled micro-pillars and (b, d, f, h) compressed micro-pillars of cold sintered and conventionally sintered ZnO.

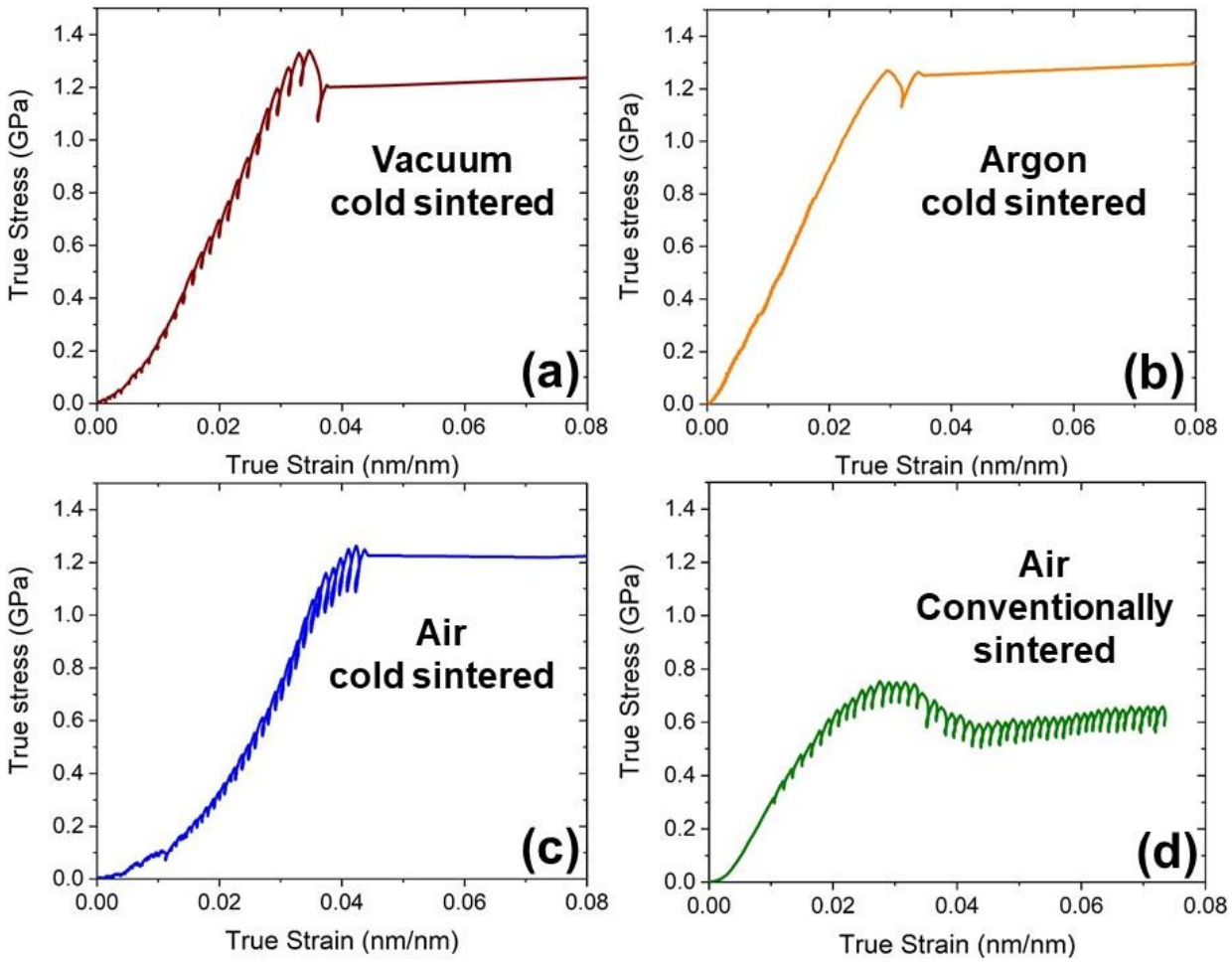

Figure 7. True stress v/s true strain curves of FIB milled micro-pillars undergone micro-compression testing using flat punch diamond indenter with a target displacement rate of 10 nm/s. These curves have been plotted for (a) vacuum, (b) argon, (c) air cold sintered samples and (d) conventionally sintered sample.

According to Lowum *et al.*, cold sintered ZnO showed a 40 % lower characteristic strength (~ 65 MPa) compared to values reported for conventionally processed ZnO (~ 120 MPa) as measured by three-point bending test mode. Concluding that no transgranular fracture occurred, as the grain boundaries were not properly bonded. [26] It is noteworthy to mention here that they used 0.8 molar aqueous solution of zinc acetate as sintering aid for ZnO. It has been debated in our previous studies that the use of acidic media might etch the grain boundaries and contribute to the formation of defects, despite the high densification. This could be a possible reason for the low strength of the cold sintered ZnO observed by Lowum *et al.*, By avoiding the use of an acidic sintering aid,

this effect can be minimized or even avoided. More generally, Guo et al. found that for cold sintered 8 YSZ sample (8YSZ = 8 mol % Y_2O_3 – stabilized ZrO_2), a conventional post sintering step was necessary after cold sintering to achieve comparable mechanical properties (Vickers hardness and fracture toughness) to that of samples prepared by other techniques. [56]

3.5 TEM investigation of deformed samples

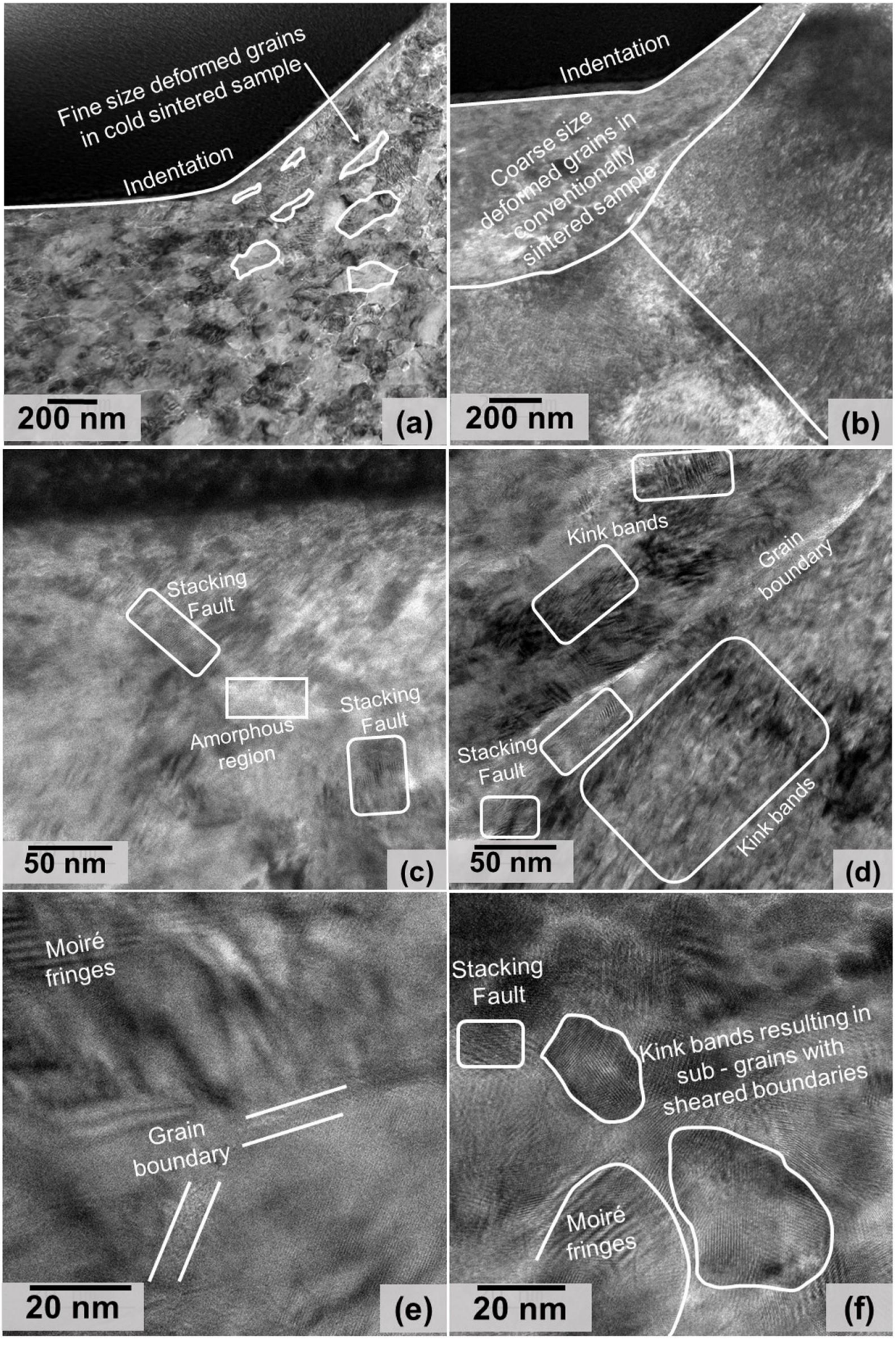
Fine size deformed grains in cold sintered sample
Indentation
200 nm
(a)
Indentation
Coarse size deformed grains in conventionally sintered sample
200 nm
(b)
Stacking Fault
Amorphous region
Stacking Fault
50 nm
(c)
Kink bands
Grain boundary
Stacking Fault
Kink bands
50 nm
(d)
Moiré fringes
Grain boundary
20 nm
(e)
Stacking Fault
Kink bands resulting in sub - grains with sheared boundaries
Moiré fringes
20 nm
(f)

Figure 8. TEM images of the deformed nanoindented region for (a, c, e) air cold sintered sample and (b, d, f) conventionally sintered sample.

Figure 8 shows the TEM investigation of the deformed regions at the flanks of the nanoindents for cold sintered (Figure 8 a, c, e) and for conventionally sintered samples (Figure 8 b, d, f). Deformed nano sized grains can be seen for cold sintered sample (Figure 8 a) and coarse sized deformed grains can be observed for conventionally sintered sample (Figure 8 b). Figure 8 c and e hints on the annihilation of preexisting stacking faults that were observed in as cold sintered sample (see Figure 2). In Figure 8 d (for conventionally sintered samples) there is an indication of the formation of kink bands resulted in sub grains with shear grain boundaries within the grains as depicted from the diffraction contrast pattern. These kink bands become even more obvious in Figure 8 f.

4. Discussion

It must be kept in consideration that the supressed grain growth of cold sintered ZnO microstructures (grain size remaining below 200 nm for samples for 20 min dwell time at 250 ^{o}C) and reasonably large grain growth for conventionally sintered ZnO (grain size > 1 μm for 60 min dwell time at 900 ^{o}C) was observed in previous studies (Figure 1). Funahashi *et al.* identified free regions in the vicinity of grain boundaries of their cold sintered ZnO as residual pores using TEM for analysis. [6] Here, use of optimized cold sintering parameters enabled us to exclude almost completely the influence of residual porosity on mechanical properties and clear triple points have been observed between grains with flat grain boundary regions (Figure 2 b, e, h). Though presence of amorphous phase (Figure 2 c, f, i) was found to be inevitable, independently of the nature of applied atmosphere during the cold sintering process. Our study delivers some new insights of specific deformation behavior of cold sintered oxides under compressive loading, which has not been reported in this detail in the literature before.

4.1 Formation of stacking faults in the as cold sintered state

Diffraction contrast fringes in Figure 2 c, f, and i clearly indicate the presence of stacking faults in the as cold sintered samples irrespective of the atmosphere used for cold sintering. TEM diffraction contrast of stacking faults is characteristically a pattern of fringes appear as light and dark fringes. [57][58] These can be observed for bended lattices from the offsets between bright and dark

fringes. Regions with difference of strain energy due to the presence of defects can be read as distribution of relaxed and strained regions caused by these defects. Normally, stacking faults appear when two adjacent planes do not lie in their proper crystallographic stacking sequence. In our previous work, XRD analysis of as received ZnO powder and also of the cold sintered sample mainly indexed the crystal structure as hexagonal wurtzite. [44] In an undisturbed wurtzite crystal, stacking sequence in the lattice is described by the sequence….AaBbAaBb…. (as Zn and O for upper case and lower case, respectively) for closely packed double layers of (0001) planes in [0001] directions. Any violation to this sequence infers a fault and which can be described as stacking fault. [59] It is interesting to compare the TEM image of as received ZnO powder (Figure S 4) that was used as starting material for cold sintering. No similar pattern could be observed for as received powder. This suggests that all observed planar defects (stacking faults) route back to the cold sintering process. For metals and its alloys, stacking faults are known to make a significant contribution to plastic deformation in the case of severe deformation, especially for face centered cubic systems. [60][61][62][63] Ceramic semiconductor materials, which belong to the Group II – IV, are known to have basal plane stacking faults. Particularly ZnO is known to have low formation energy for stacking faults thereby it is likely to found such defects in its crystal structure. [59] In literature several times, stacking faults have been discussed for ZnO, for instance during growth of films, during field assisted sintering and others. [64][38][64]

In the present case, it can be inferred that the use of high external pressure and wetting of primary particles with aqueous cold sintering aid helped in the formation of these stacking faults in the as cold sintered samples. As explained by the mechanisms of cold sintering, use of compatible cold sintering aqueous phase at grain boundary areas with the assistance of high external pressures, facilitate dissolution – precipitation mechanism and develops chemical potentials of charge carriers. Hereby, exchange of atoms/ions takes place and contribute to the shift of energy demands from high temperature sintering towards low temperature sintering. This mechanism helped also in explaining the presence of amorphous regions at grain boundary areas which then can be optionally crystallized by post thermal treatments. The mechanism explained so far in the literature also support the fact that this exchange of ions at grain boundary regions would contribute towards defect formation altering their concentration. [2][10][3] Formation of oxygen – hydrogen related defects has also been confirmed for ZnO in the presence of water (adsorbed on its surface). [65]

This has been discussed in detail by Gonzalez et al. resulting in appearance of protonated disorder at grain boundary regions during cold sintering of ZnO. A detailed analysis and calculation of stress exponent to be 2 – 4 suggested the role of plastic deformation as one of the active mechanisms for achieving high densification during cold sintering. [8] Presence of aqueous phase at grain boundary regions could be helping in assisting the nucleation of these stacking faults by providing a source of atoms/ions. For flash sintered ZnO, formation of stacking faults have been observed as well. In this case, these were preferentially formed within the grains rather than at grain boundaries. This effect was explained that grain boundaries act as a sink for oxygen vacancies. [64] While for cold sintering, an opposite behavior was observed highlighting the role of aqueous phase in generating these defects.

4.2 Mechanical properties of cold sintered ZnO

A comparison of the mechanical properties between our samples with that of literature has been depicted in Table 1.

Table 1. Comparison of the hardness and elastic moduli of polycrystalline ZnO obtained in the present study compared to those reported in literature. All data were obtained using nanoindentation testing.

ZnO	Technique of preparation	Hardness (GPa)	Elastic Modulus (GPa)	Penetration depth (nm)	Reference
Polycrystalline ZnO	Cold sintering	5.5 ± 0.5	100 ± 5	45 mN target load penetration ~ 900 nm	Present study
	Conventional sintering	4.8 ± 0.6	109 ± 6	45 mN target load penetration ~ 1000 nm	
ZnO single crystal	Commercial ZnO single crystal (0001) oriented	5.0 ± 0.1	111.2 ± 4.7	300	[30]

Single crystal	Commercial ZnO single crystal (0001 oriented)	5.4 ± 0.7	112.5 ± 8.4		[31]
ZnO single crystal	Hexagonal wurtzite structure grown by seeded chemical vapour transport (0001), $(000\bar{1})$, $(10\bar{1}0)$	2 to 8	104 – 134	150	[32]
ZnO single crystal	-	6.6 ± 0.1	131.2 ± 2.6	~ 1000 nm	[37]
Nanocrystalline ZnO	Conventional sintering at 500 and 700 ^{o}C	4 – 7	100	-	[66]
ZnO single crystal and poly crystal	Ab Initio calculations		Single crystal = 121 Poly crystal = 116	-	[67]

A comparison of the deformation of these cold sintered and the conventionally sintered samples shows that the difference in the deformation behaviour is very likely related to the different grain sizes. Grain boundary sliding is one of the common deformation modes of nano-crystalline and ultrafine grained materials, at room temperature [68][69][70][52][53] and is also a common cause of pile up in such materials. Maier et al. [70] observed grain boundary sliding causing the formation of pile ups around indents in ultra-fine grained aluminium and related it to the unconstrained surface grains. Wang et al. [52] also observed larger pile ups around indents in nano-grained Yttrium Aluminium Garnet ($Y_3Al_5O_{12}$, YAG) transparent ceramics in comparison to coarse-grained YAG ceramics. They proposed grain boundary sliding as the predominant deformation mode in nano-grained YAG ceramics [52][53]. In the present work, it is assumed that the pile ups observed around the indents in nano crystalline ZnO (Figure 3 a, b. c) are caused by grain boundary sliding occurring in the unconstrained surface grains. This phenomenon was not observed when it was easier for grains to be displaced in their vicinity because of large degree of porosity (Figure S

2). These pores resulted due to excessive removal of particles in case of harsh environment of grinding/polishing with even intensified effect for large size particles in conventionally sintered sample. Therefore, improvised surface preparation technique was favoured and only these samples (Figure 3) were selected for nanoindentation and detailed TEM investigation. In the case of conventionally sintered samples, no material pile ups around the indents were observed.

As the density for both (cold and conventionally sintered) samples is nearly identical, the slightly lower elastic modulus observed for cold sintered ZnO is assumed to be related to its fine grain size. Fine grained and nano crystalline materials have higher volume fractions of grain boundaries than coarse grained microstructures. As shown by TEM investigation, amorphous layers are also located at the grain boundaries in the ZnO cold sintered samples. These are supposed to possess a lower density and elastic modulus than the crystalline grains. [52][53][50] However, there could be additional influences such as different interatomic bonding or varying defect concentrations at or nearby to these areas. All elastic modulus values are very close to the values of bulk ZnO single crystals and also of high temperature conventionally sintered ZnO (polycrystal) keeping in mind the influence of pile – up, as can be seen in Table 1.

In case of micro compression testing, presence of pores, on the surface of the micro-pillar, which are preferentially located at grain boundaries or triple junctions (Figure 6 g) are assumed to act as weakening points or stress concentrations. On the other hand, both type of samples, cold sintered and conventionally sintered, have the same amount of porosity, as calculated by Archimedes density measurements. Thereby it can be said at this point that these pores are very tiny and well distributed in cold sintered sample, while in conventionally sintered samples, high temperature formed pore coalescence. Besides that, the conventionally sintered ZnO shows some amount of damage (micro – cracking) as evident from the stress drop *Figure 7* d. This is also evident from the SEM image of the deformed micro-pillar in Figure 6 h revealing intergranular fracture. We assume that some plastic deformation might have occurred before failure occurred by intergranular fracture in the coarse grained conventionally sintered sample. Therefore, no easy short crack path across the pillar exists and the crack gets deflected along the grain boundaries. This might cause an extrinsic toughening effect as stress has to be applied to move the cracks through the pillar.

On the other hand, we could show in a recent study [25] that the cold sintered samples are in a way to minimize pores in the cold sintered ZnO microstructure. This is further revealed in the TEM

images of the cold sintered samples (Figure 2 b, e, h) where pore-free triple points were observed. Even after sintering at 900 ^{o}C for one hour in case of conventional sintering, it was not possible to generate a microstructure with pore-free triple points as were achieved for the cold sintered samples at 250 ^{o}C with only 20 min dwell time. We assume that by removing the amorphous films that formed at the grain boundaries during cold sintering the mechanical response could be even improved.

A detailed comparison for compressive stress of ZnO between present studies and that of literature has been made in Table 2. Sung *et al.,* used a ZnO wafer (prepared by the hydrothermal method, c – plane orientation) to FIB mill micro-pillars for compression testing. They reported a compressive stress of 3 GPa (with 6 % strain) for as – milled ZnO micro-pillars and a yield stress of 2 GPa (with 10 % strain) for annealed ZnO micro-pillars. [36] These documented values are almost comparable to the compressive stress of cold sintered samples. In present studies, small grains in cold sintered samples, each having their distinct crystallographic orientations (each grain act as a single crystal) respond accordingly to applied compressive loads. Thereby, cumulative response of active/non-active slip systems, provided by favorable and unfavorable planes would result in higher value of compressive stress for cold sintered samples. Furthermore, dislocation densities are highly affected by amount of grain boundary areas, in terms of entangling together or bursting out during compressive loading. [31][36]

Table 2. Comparison of compressive stress for ZnO observed in present studies with that of literature.

ZnO	Type of compression testing	Maximum compressive stress	Reference
polycrystalline ZnO Cold sintered	Micro-compression test on micro-pillars of ~ 2 µm diameter and ~ 3 – 4 µm length	1.2 GPa	Present study
Conventionally sintered		0.8 GPa	
ZnO wafer	Micro compression test on micro-pillars of ~ 1 µm in diameter and 2.4 µm in height	2 – 3 GPa	[36]

ZnO single crystal	Micro-compression test on micro-pillars with diameter to height ratio below 1:3 (diameters = 100 nm to 700 nm)	Onset of shearing = 0.5 mN for 300 nm diameter micro-pillar and 3.5 mN for 500 nm diameter micro-pillar.	[37]
Flash sintered ZnO (95 % dense at 700 ^{o}C with grain size of 1.3 $\pm$ 0.3 µm on positive side and 1.2 $\pm$ 0.3 µm on negative side)	Micro-compression testing on the micro-pillars (~ 3 µm in diameter and ~ 8 µm in height) of the positive side of the flash sintered ZnO	Flow stress of 1.21 GPa at a strain rate of 8 % for room temperature micro compression	[38]
Conventionally sintered ZnO (94 % dense at 1100 ^{o}C with grain size 1.7 $\pm$ 0.6 µm)	Micro-compression testing on micro-pillars ~ 3 µm in diameter and ~ 8 µm in height.	Flow stress of ~ 0.94 GPa.	

However, a better comparison can be made with the work of Cho et al., who did in-situ micro-compression testing on flash sintered ZnO (grain size = 1.3 $\pm$ 0.3 µm) and conventionally sintered ZnO (grain size = 1.7 $\pm$ 0.3 µm). For room temperature micro-compression testing, they observed 1.19 GPa (strain of 8 %) for flash sintered micro-pillars and 0.9 GPa (strain of 5 %) for conventionally sintered micro-pillar accompanied by intergranular fracture. Despite of very negligible difference in the grain sizes for both samples, the difference in the values of yield stress was explained on the basis of high density dislocations near grain boundaries. [38]

4.3 Role of preexisting stacking faults on deformation of cold sintered ZnO

To study the influence of preexisting defects observed in cold sintered samples (Figure 2 c, f, i), towards the mechanical properties, TEM investigation on samples deformed by nanoindentation was conducted as well. Nano sized grains in cold sintered samples (Figure 1 c) were observed to be deformed in the direction perpendicular to the applied compressive load (Figure 8 a). Preexisting stacking faults seem to become annihilated in the highly deformed regions at the flanks of the nanoindents (Figure 8 b and c). This annihilation could be because of major sinks present in

the form of large number of grain boundaries and also the amorphous regions. Preexisting dislocations in ceramic materials have been discussed to assist in better energy absorption of compressive loading. [71] In the present work, this special kind of annihilation of preexisting stacking faults obviously helped the cold sintered structure to absorb the compressive loading easily assisting plastic deformation without localization of the plastically deformed regions. Hence, clearly pronounced materials pile up without cracking has been observed

Figure 3 3 c. Here amorphous phase could also be a contributing factor in assisting this plastic flow as explained earlier. On the contrary, diffraction contrast pattern observed for conventionally sintered samples indicates the formation of kink bands as additional deformation mechanism (Figure 8 d). Kink bands are known as indication of shear localization phenomenon observed particularly for anisotropic materials like lamellar structures and composites. [72] They are described as gliding of layered structure accompanied by external rotation. [73] Kink bands were firstly observed for Cadmium and explained as elastic buckling of basal slip planes resulting in an instability of the crystal. This happens when large stress is loaded parallel to these slip planes. [74][75] These kinks are known to accommodate stress and might become the main reason for cracking and delamination of anisotropic materials and layered ceramics. [75][76] Polycrystalline systems, particularly hexagonal closely packed systems like wurzite, where only 3 basal slip system are active, endure strong plastic anisotropy and therefore facilitate kink formation. [77] In the present study, anisotropic crystal orientation of coarse grains in conventionally sintered samples (Figure 8 a) can explain the development of kink bands under compressive nanoindentation loading (Figure 8 a) resulting in sub grains with sheared grain boundaries (Figure 8 f). This in turn adds more to anisotropy and makes it difficult for coarse grains with sub – grains within, to flow easily under compressive nanoindentation loading. Therefore, cracking can be observed in the vicinity of nanoindents. According to this explanation, even more anisotropy must be expected in nano-crystalline cold sintered ZnO, but for these samples, role of preexisting stacking faults probably in combination with grain boundary sliding helped in avoiding localized plastic shearing. Conclusions based on nanoindentation tests are supported by the related micro-pillar tests showing a more or less homogeneous deformation of the cold sintered pillar without fragmentation in singular pieces (Figure 6 f), while deformation of conventionally sintered ZnO is characterized by intergranular fracture (Figures 6 h).

Conclusions

A systematic study was made to investigate the mechanical response of cold sintered homogenous dense ZnO structures on the level of individual grains. Samples in the present work were, cold sintered with 98 – 99 % relative density having grain sizes < 200 nm and almost pore-free grain boundaries. There were observed formation of amorphous films and nucleation of planar defects such as stacking faults, at and in the vicinity of the grain boundaries by TEM analysis of as cold sintered samples. Mechanical properties of cold sintered ZnO prepared in three different atmospheres were investigated using nanoindentation and micro-pillar compression tests. Using nanoindentation, with a visible pile – up, a hardness of ~ 100 $\pm$ 5 and an elastic modulus 5.5 GPa $\pm$ 0.5 GPa was measured for all three cold sintered samples. No influence of the applied atmosphere was observed on the cold sintered microstructure, densification and their response to the compressive loading. These values were found to be almost comparable to the documented values in the literature even though the effect of pile – up was not corrected for. Furthermore, these values are comparable to those of conventionally sintered samples where a hardness of 4.8 GP ± 0.6 and an elastic modulus of 109 GPa $\pm$ 6 was obtained. Beside that a higher scatter in the data for conventionally sintered samples was observed to be due to larger heterogeneity in samples. Preexisting stacking faults were observed to play their role in assisting the mechanical response of cold sintered samples as observed by TEM investigation of deformed nanoindented regions.

Micro-pillar testing of the three cold sintered samples also showed identical compressive strength (1.2 GPa) independent of the synthesis atmosphere. The micro-compression strength of the conventionally sintered sample amounted to about 0.8 GPa, i.e. significantly lower than that of cold sintered ZnO. The lower strength is assumed to be caused by residual porosity at the grain boundaries. The compressive strength of cold sintered ZnO were observed to be comparable to that of ZnO single crystals despite of the very low sintering temperature. Therefore, it can be concluded that an optimum selection of the cold sintering parameters is the key to reduce residual pits/pores at grain boundary regions and also to introduce a better energy absorbing effect to finally achieve mechanical properties competing or even better with the bulk properties.

We demonstrated that nanoindentation and micro-pillar testing are promising characterization methods for studying the mechanical response of cold sintered samples enabling better understanding and interpretation on the relationship between the microstructure in the as cold

sintered state and the resulting mechanical properties. Up to now, clear understanding of how the individual grains in cold sintered ceramics interact with each other under an applied load and understanding of the role of dislocations and stacking faults was largely missing. Present studies could be considered as preliminary initiative to have a clear understanding of mechanical behavior for these appreciably low temperature sintered microstructures and a descriptive detail that can help in future for improving the cold sintering process to the commercial level. Finally, it should be mentioned that nanoindentation and micropillar tests cannot replace macroscopic deformation tests, which are necessarily required for evaluating the potential of cold sintered samples if an application as structural parts is aspired.

Acknowledgements

Khushnuda Nur and Muhammad Zubair acknowledge the funding from the German Research Foundation (DFG) through projects GU993/10 and SFB1394 (sub-project C02; project number 409476157), respectively, and also the support from University of Engineering and Technology, Lahore, Pakistan. We are very grateful for the help and support provided by Prof. Dr. Sandra Korte-Kerzel. Special thanks go to Mr. Mark Kappertz for his help in ceramographic preparation of samples for micro-pillar tests. Furthermore, we would like to thank Mr. Maximilian Kruth, Zheng Ma, Kevin Kistermann, Sebastian Zischke and Prof. Dr. Thomas E. Weirich for their support in TEM imaging.

Conflicts of interest

There are no conflicts of interest.

References

[1] J. Guo, S. S. Berbano, H. Guo, A. L. Baker, M. T. Lanagan, and C. A. Randall, “Cold Sintering Process of Composites: Bridging the Processing Temperature Gap of Ceramic and Polymer Materials,” *Adv. Funct. Mater.*, vol. 26, no. 39, pp. 7115–7121, 2016.

[2] J. Guo *et al.*, “Cold Sintering: A Paradigm Shift for Processing and Integration of Ceramics,” *Angew. Chemie - Int. Ed.*, vol. 55, no. 38, pp. 11457–11461, 2016.

[3] M. Biesuz *et al.*, “A theoretical analysis of cold sintering,” *Adv. Appl. Ceram.*, vol. 119, no. 2, pp. 75–89, 2020.

[4] S. Grasso *et al.*, “A review of cold sintering processes,” *Adv. Appl. Ceram.*, vol. 119, no. 3, pp. 115–143, 2020.

[5] Z. M. Grady, K. Tsuji, A. Ndayishimiye, J. Hwan-Seo, and C. A. Randall, "Densification of a Solid-State NASICON Sodium-Ion Electrolyte below 400 °c by Cold Sintering with a Fused Hydroxide Solvent," *ACS Appl. Energy Mater.*, vol. 3, no. 5, pp. 4356–4366, 2020.

[6] S. Funahashi *et al.*, "Demonstration of the cold sintering process study for the densification and grain growth of ZnO ceramics," *J. Am. Ceram. Soc.*, vol. 100, no. 2, pp. 546–553, 2017.

[7] X. Kang, R. Floyd, S. Lowum, D. Long, E. Dickey, and J. P. Maria, "Cold sintering with dimethyl sulfoxide solutions for metal oxides," *J. Mater. Sci.*, vol. 54, no. 10, pp. 7438–7446, 2019.

[8] J. Gonzalez-Julian *et al.*, "Unveiling the mechanisms of cold sintering of ZnO at 250 °C by varying applied stress and characterizing grain boundaries by Kelvin Probe Force Microscopy," *Acta Mater.*, vol. 144, pp. 116–128, 2018.

[9] H. Guo, J. Guo, A. Baker, and C. A. Randall, "Cold sintering process for ZrO2-based ceramics: significantly enhanced densification evolution in yttria-doped ZrO2," *J. Am. Ceram. Soc.*, 2017.

[10] H. Guo, A. Baker, J. Guo, and C. A. Randall, "Cold Sintering Process: A Novel Technique for Low-Temperature Ceramic Processing of Ferroelectrics," *J. Am. Ceram. Soc.*, vol. 99, no. 11, pp. 3489–3507, 2016.

[11] H. Kähäri, M. Teirikangas, J. Juuti, and H. Jantunen, "Dielectric Properties of Lithium Molybdate Ceramic Fabricated at Room Temperature," *J. Am. Ceram. Soc.*, vol. 97, no. 11, pp. 3378–3379, 2014.

[12] and H. J. Hanna Kähöri, Merja Teirikangas, Jari Juuti, "Improvements and Modifications to Room-Temperature Fabrication Method for Dielectric Li 2 MoO 4 Ceramics," vol. 689, pp. 687–689, 2015.

[13] A. Baker, H. Guo, J. Guo, C. Randall, and D. J. Green, "Utilizing the Cold Sintering Process for Flexible–Printable Electroceramic Device Fabrication," *J. Am. Ceram. Soc.*, vol. 99, no. 10, pp. 3202–3204, 2016.

[14] J. P. Maria *et al.*, "Cold sintering: Current status and prospects," *J. Mater. Res.*, vol. 32, no. 17, pp. 3205–3218, 2017.

[15] J. H. Seo *et al.*, "Cold sintering approach to fabrication of high rate performance binderless LiFePO4 cathode with high volumetric capacity," *Scr. Mater.*, vol. 146, pp. 267–271, 2018.

[16] J. H. Seo *et al.*, "Broad temperature dependence, high conductivity, and structure-property relations of cold sintering of LLZO-based composite electrolytes," *J. Eur. Ceram. Soc.*, vol. 40, no. 15, pp. 6241–6248, 2020.

[17] H. Guo, J. Guo, A. Baker, and C. A. Randall, "Hydrothermal-Assisted Cold Sintering Process: A New Guidance for Low-Temperature Ceramic Sintering," *ACS Appl. Mater. Interfaces*, vol. 8, no. 32, pp. 20909–20915, 2016.

[18] Y. D. Ivakin *et al.*, "Cold Sintering of ZnO Ceramic in Water Medium: Test

Demonstration," *Glas. Ceram. (English Transl. Steklo i Keramika)*, vol. 76, no. 5–6, pp. 210–215, 2019.

[19] Y. Jing *et al.*, "Remarkably improved electrical conductivity of ZnO ceramics by cold sintering and post-heat-treatment," *Ceram. Int.*, vol. 44, no. 16, pp. 20570–20574, 2018.

[20] H. Leng, J. Huang, J. Nie, and J. Luo, "Cold sintering and ionic conductivities of Na3.256Mg0.128Zr1.872Si2PO12solid electrolytes," *J. Power Sources*, vol. 391, no. February, pp. 170–179, 2018.

[21] J. G. Pereira da Silva *et al.*, "Sintering of a sodium-based NASICON electrolyte: A comparative study between cold, field assisted and conventional sintering methods," *J. Eur. Ceram. Soc.*, vol. 39, no. 8, pp. 2697–2702, 2019.

[22] W. A. Soer, K. E. Aifantis, and J. T. M. De Hosson, "Incipient plasticity during nanoindentation at grain boundaries in body-centered cubic metals," *Acta Mater.*, vol. 53, no. 17, pp. 4665–4676, 2005.

[23] Y. L. Shen, *Nanoindentation for testing material properties*. 2019.

[24] M. J. Mayo, R. W. Siegel, and W. D. Nix, "Mechanical Properties of Nanophase TiO2 as Determined by Nanoindentation," *J. Mater. Res.*, vol. 5, no. 5, pp. 1073–1082, 1990.

[25] K. Nur, T. P. Mishra, J. G. P. da Silva, J. Gonzalez-Julian, M. Bram, and O. Guillon, "Influence of powder characteristics on cold sintering of nano-sized ZnO with density above 99 %," *J. Eur. Ceram. Soc.*, vol. 41, no. 4, pp. 2648–2662, 2021.

[26] S. Lowum, R. Floyd, R. Bermejo, and J. P. Maria, "Mechanical strength of cold-sintered zinc oxide under biaxial bending," *J. Mater. Sci.*, vol. 54, no. 6, pp. 4518–4522, 2019.

[27] A. Fischer-Cripps, and D. Nicholson, *Nanoindentation. Mechanical Engineering Series*, vol. 57, no. 2. 2004.

[28] M. D. Uchic and D. M. Dimiduk, "A methodology to investigate size scale effects in crystalline plasticity using uniaxial compression testing," *Mater. Sci. Eng. A*, vol. 400–401, no. 1-2 SUPPL., pp. 268–278, 2005.

[29] S. Korte-Kerzel, "Microcompression of brittle and anisotropic crystals: Recent advances and current challenges in studying plasticity in hard materials," *MRS Commun.*, vol. 7, no. 2, pp. 109–120, 2017.

[30] S. O. Kucheyev, J. E. Bradby, J. S. Williams, C. Jagadish, and M. V. Swain, "Mechanical deformation of single-crystal ZnO," *Appl. Phys. Lett.*, vol. 80, no. 6, pp. 956–958, 2002.

[31] S. R. Jian, "Mechanical responses of single-crystal ZnO," *J. Alloys Compd.*, vol. 494, no. 1–2, pp. 214–218, 2010.

[32] D. A. Lucca, M. J. Klopfstein, R. Ghisleni, and G. Cantwell, "Investigation of Polished Single Crystal ZnO by Nanoindentation," *CIRP Ann.*, vol. 51, no. 1, pp. 483–486, 2002.

[33] R. Navamathavan *et al.*, "A nanoindentation study of the mechanical properties of ZnO thin films on (0 0 0 1) sapphire," *Appl. Surf. Sci.*, vol. 253, no. 2, pp. 464–467, 2006.

[34] T. H. Fang, W. J. Chang, and C. M. Lin, “Nanoindentation characterization of ZnO thin films,” *Mater. Sci. Eng. A*, vol. 452–453, pp. 715–720, 2007.

[35] R. Navamathavan, S. J. Park, J. H. Hahn, and C. K. Choi, “Nanoindentation ‘pop-in’ phenomenon in epitaxial ZnO thin films on sapphire substrates,” *Mater. Charact.*, vol. 59, no. 4, pp. 359–364, 2008.

[36] T. H. Sung, J. C. Huang, J. H. Hsu, S. R. Jian, and T. G. Nieh, “Yielding and plastic slip in ZnO,” *Appl. Phys. Lett.*, vol. 100, no. 21, pp. 12–16, 2012.

[37] A. Rinaldi, R. Araneo, M. Pea, and A. Notargiacomo, “Observations of nanoscale properties of ZnO pillars subject to compression,” *IEEE-NANO 2015 - 15th Int. Conf. Nanotechnol.*, pp. 518–521, 2015.

[38] J. Cho *et al.*, “Temperature effect on mechanical response of flash-sintered ZnO by in-situ compression tests,” *Acta Mater.*, vol. 200, pp. 699–709, 2020.

[39] D. Meertens, M. Kruth, and K. Tillmann, “FEI Helios NanoLab 400S FIB-SEM,” *J. large-scale Res. Facil. JLSRF*, vol. 2, pp. 3–6, 2016.

[40] M. Luysberg, M. Heggen, and K. Tillmann, “FEI Tecnai G2 F20,” *J. large-scale Res. Facil. JLSRF*, vol. 2, pp. 2–5, 2016.

[41] H. Fei, A. Abraham, N. Chawla, and H. Jiang, “Evaluation of micro-pillar compression tests for accurate determination of elastic-plastic constitutive relations,” *J. Appl. Mech. Trans. ASME*, vol. 79, no. 6, 2012.

[42] W. C. Oliver and G. M. Pharr, “Measurement of hardness and elastic modulus by instrumented indentation: Advances in understanding and refinements to methodology,” *J. Mater. Res.*, vol. 19, no. 1, pp. 3–20, 2004.

[43] M. Y. Soomro, I. Hussain, N. Bano, E. Broitman, O. Nur, and M. Willander, “Nanoscale elastic modulus of single horizontal ZnO nanorod using nanoindentation experiment,” pp. 1–5, 2012.

[44] K. Nur, T. Prasad, J. Gonzalez-julian, M. Bram, and O. Guillon, “Inluence of powder characteristics on cold sintering of nano-sized ZnO with density above 99 %,” vol. 41, no. October 2020, pp. 2648–2662, 2021.

[45] M. A. G. Maneiro and J. Rodríguez, “Pile-up effect on nanoindentation tests with spherical-conical tips,” *Scr. Mater.*, vol. 52, no. 7, pp. 593–598, 2005.

[46] D. Zhang, L. G. Zhao, A. Roy, and Y. L. Chiu, “Nanoscale investigation of deformation characteristics in a polycrystalline silicon carbide,” *J. Aust. Ceram. Soc.*, vol. 56, no. 3, pp. 951–967, 2020.

[47] M. Becton and X. Wang, “Grain-size dependence of mechanical properties in polycrystalline boron-nitride: A computational study,” *Phys. Chem. Chem. Phys.*, vol. 17, no. 34, pp. 21894–21901, 2015.

[48] J. Zhou, Y. Li, R. Zhu, and Z. Zhang, “The grain size and porosity dependent elastic moduli and yield strength of nanocrystalline ceramics,” *Mater. Sci. Eng. A*, vol. 445–446,

pp. 717–724, 2007.

[49] M. Weller, J. Diehl, and H. E. Schaefer, “Shear modulus and internal friction in nanometre-sized polycrystalline palladium,” *Philos. Mag. A Phys. Condens. Matter, Struct. Defects Mech. Prop.*, vol. 63, no. 3, pp. 527–533, 1991.

[50] O. Yeheskel, R. Chaim, Z. Shen, and M. Nygren, “Elastic moduli of grain boundaries in nanocrystalline MgO ceramics,” *J. Mater. Res.*, vol. 20, no. 3, pp. 719–725, 2005.

[51] R. Chaim and M. Hefetz, “Effect of grain size on elastic modulus and hardness of nanocrystalline ZrO2-3 wt% Y2O3 ceramic,” *J. Mater. Sci.*, vol. 39, no. 9, pp. 3057–3061, 2004.

[52] H. M. Wang *et al.*, “Unique mechanical properties of nano-grained YAG transparent ceramics compared with coarse-grained partners,” *Mater. Des.*, vol. 105, pp. 9–15, 2016.

[53] H. Wang, R. Li, M. Zhou, J. Cedelle, Z. Huang, and Q. Wang, “Grain boundary sliding mechanism in plastic deformation of nano-grained YAG transparent ceramics: Generalized self-consistent model and nanoindentation experimental validation,” *J. Eur. Ceram. Soc.*, vol. 37, no. 7, pp. 2705–2715, 2017.

[54] C. Q. Chen, Y. Shi, Y. S. Zhang, J. Zhu, and Y. J. Yan, “Size dependence of Young’s modulus in ZnO nanowires,” *Phys. Rev. Lett.*, vol. 96, no. 7, pp. 1–4, 2006.

[55] H. S. Kim and M. B. Bush, “Effects of grain size and porosity on the elastic modulus of nanocrystalline materials,” *Nanostructured Mater.*, vol. 11, no. 3, pp. 361–367, 1999.

[56] H. Guo, T. J. M. Bayer, J. Guo, A. Baker, and C. A. Randall, “Cold sintering process for 8 mol%Y2O3-stabilized ZrO2ceramics,” *J. Eur. Ceram. Soc.*, vol. 37, no. 5, pp. 2303–2308, 2017.

[57] B. Fultz and J. Howe, “Diffraction Contrast in TEM Images,” pp. 349–427, 2013.

[58] D. Hull and D. J. Bacon, “Observation of Dislocations,” *Introd. to Dislocations*, no. 2, pp. 21–41, 2011.

[59] Y. Yan, G. M. Dalpian, M. M. Al-Jassim, and S. H. Wei, “Energetics and electronic structure of stacking faults in ZnO,” *Phys. Rev. B - Condens. Matter Mater. Phys.*, vol. 70, no. 19, pp. 1–4, 2004.

[60] W. W. Jian *et al.*, “Physics and model of strengthening by parallel stacking faults,” *Appl. Phys. Lett.*, vol. 103, no. 13, 2013.

[61] Y. L. Gong *et al.*, “Simultaneously enhanced strength and ductility of Cu-xGe alloys through manipulating the stacking fault energy (SFE),” *Mater. Sci. Eng. A*, vol. 569, pp. 144–149, 2013.

[62] V. S. Sarma *et al.*, “Role of stacking fault energy in strengthening due to cryo-deformation of FCC metals,” *Mater. Sci. Eng. A*, vol. 527, no. 29–30, pp. 7624–7630, 2010.

[63] K. Youssef, M. Sakaliyska, H. Bahmanpour, R. Scattergood, and C. Koch, “Effect of stacking fault energy on mechanical behavior of bulk nanocrystalline Cu and Cu alloys,” *Acta Mater.*, vol. 59, no. 14, pp. 5758–5764, 2011.

[64] X. L. Phuah *et al.*, “Comparison of the grain growth behavior and defect structures of flash sintered ZnO with and without controlled current ramp,” *Scr. Mater.*, vol. 162, pp. 251–255, 2019.

[65] B. Dargatz, J. Gonzalez-Julian, M. Bram, Y. Shinoda, F. Wakai, and O. Guillon, “FAST/SPS sintering of nanocrystalline zinc oxide-Part II: Abnormal grain growth, texture and grain anisotropy,” *J. Eur. Ceram. Soc.*, vol. 36, no. 5, pp. 1221–1232, 2016.

[66] W. D. Nix and R. W. Siegel, “Nanoindentation of nanocrystalline ZnO,” *J. Mater. Res.*, vol. 7, no. 4, pp. 973–979, 1992.

[67] I. R. Shein, V. S. Kiĭko, Y. N. Makurin, M. A. Gorbunova, and A. L. Ivanovskiĭ, “Elastic parameters of single-crystal and polycrystalline wurtzite-like oxides BeO and ZnO: Ab initio calculations,” *Phys. Solid State*, vol. 49, no. 6, pp. 1067–1073, 2007.

[68] N. Q. Chinh, P. Szommer, T. Csanádi, and T. G. Langdon, “Flow processes at low temperatures in ultrafine-grained aluminum,” *Mater. Sci. Eng. A*, vol. 434, no. 1–2, pp. 326–334, 2006.

[69] N. Q. Chinh, T. Csanádi, J. Gubicza, R. Z. Valiev, B. B. Straumal, and T. G. Langdon, “The effect of grain boundary sliding and strain rate sensitivity on the ductility of ultrafine-grained materials,” *Mater. Sci. Forum*, vol. 667–669, pp. 677–682, 2011.

[70] V. Maier, B. Merle, M. Göken, and K. Durst, “An improved long-term nanoindentation creep testing approach for studying the local deformation processes in nanocrystalline metals at room and elevated temperatures,” *J. Mater. Res.*, vol. 28, no. 9, pp. 1177–1188, 2013.

[71] L. Porz *et al.*, “Dislocation-toughened ceramics,” *Mater. Horizons*, vol. 8, no. 5, pp. 1528–1537, 2021.

[72] T. J. Nizolek, T. M. Pollock, and R. M. McMeeking, “Kink band and shear band localization in anisotropic perfectly plastic solids,” *J. Mech. Phys. Solids*, vol. 146, no. July 2019, p. 104183, 2021.

[73] F.HOERZ, “Static and Dynamic Origin of Kink Bands in Micas,” *J Geophys Res*, vol. 75, no. 5, pp. 965–977, 1970.

[74] B. E. Orowan, “Nature 643,” no. 3788, pp. 643–644, 1942.

[75] K. Hagihara, N. Yokotani, and Y. Umakoshi, “Plastic deformation behavior of Mg12YZn with 18R long-period stacking ordered structure,” *Intermetallics*, vol. 18, no. 2, pp. 267–276, 2010.

[76] X. W. Lei and A. Nakatani, “Analysis of kink deformation and delamination behavior in layered ceramics,” *J. Eur. Ceram. Soc.*, vol. 36, no. 9, pp. 2311–2317, 2016.

[77] A. Marano, L. Gélébart, and S. Forest, “FFT-based simulations of slip and kink bands formation in 3D polycrystals: Influence of strain gradient crystal plasticity,” *J. Mech. Phys. Solids*, vol. 149, 2021.